IEEE Access
Multidisciplinary | Rapid Review | Open Access Journal

SPECIAL SECTION ON GREEN SIGNAL PROCESSING FOR WIRELESS COMMUNICATIONS AND NETWORKING

Received December 11, 2018, accepted January 15, 2019, date of publication January 23, 2019, date of current version February 12, 2019.

Digital Object Identifier 10.1109/ACCESS.2019.2894733

Strategy-Based Gain Ratio Power Allocation in Non-Orthogonal Multiple Access for Indoor Visible Light Communication Networks

SIYU TAO, (Student Member, IEEE), HONGYI YU, QING LI, AND YANQUN TANG
National Digital Switching System Engineering and Technological Research Center, Zhengzhou 450001, China

Corresponding author: Hongyi Yu (xxgcmaxyu@163.com)

This work was supported in part by the National Natural Science Foundations of China under Grant 61601516 and Grant 61671477.

ABSTRACT Visible light communication (VLC) is an evolving green communication technology for indoor wireless communication networks. VLC utilizes light-emitting diodes (LEDs) for both illumination and communication. To achieve economic and energy-efficient communications, non-orthogonal multiple access (NOMA) improves the system throughput by enhancing spectral efficiency. In indoor VLC networks, the gain ratio power allocation (GRPA) of NOMA allocates greater signal power to the users of poor channels to achieve both fairness and high data rate. However, current GRPA strategies developed for radio frequency channels are not necessarily effective in all VLC channel and illumination cases. This study makes the following contributions. First, a GRPA strategy based on VLC channels is proposed that modifies the power counting and channel proportions enhance the NOMA-VLC throughput. Second, owing to difficulties of directly analyzing NOMA-VLC throughput, an alternative lower bound based on a VLC channel model to facilitate throughput comparisons is proposed. It is proved that the proposed alternative lower bound is asymptotic and compact with respect to NOMA-VLC throughput. Third, for the case of LED heights greater than 1 m, a local extremum solution using the proposed strategy is analytically demonstrated based on the alternative bound of VLC network throughput. Then, for the case of LED heights smaller than 1 m, the necessary but not sufficient condition under which the proposed strategy outperforms previous strategies is provided in VLC scenarios. Finally, the experimental results demonstrate the compactness of the proposed alternate lower bound and the advantages of the proposed strategy.

INDEX TERMS Visible light communication, non-orthogonal multiple access, gain ratio power allocation, illumination scenario.

I. INTRODUCTION

According to the Cisco Visual Networking Index [1], 80% of Internet traffic will become video, requiring high-speed wireless communication at an average speed of 20 megabits per second (Mbps). If demand increases as expected and the Internet of Things (IoT) becomes a reality, the number of connected devices will grow from 5 billion to over 20 billion by 2020. Because billions of new wireless devices are expected to be added to the Internet in the coming decade, wireless devices including smartphones and IoT equipment will consume a significant amount of power and substantial global greenhouse gas emissions will be produced by new infrastructure. However, in the next generation of wireless communication, visible light communication (VLC) [2] is a promising technology for advanced green-oriented networks [3]. VLC utilizes light emitting diodes (LEDs) to offer the wireless transmission of data in the license-free radio spectrum. Common LED bulbs consume 85% less energy than their incandescent counterparts, and their deployment is poised to have a massive impact on the energy mix, with lighting currently accounting for as much as 15% of global electricity consumption and 5% of worldwide greenhouse gas emissions [4]. Furthermore, the LEDs that could be considered as access points (APs) for serving mobile users are ubiquitous in daily lives and applicable to both general lighting and wireless communication. Massive numbers of energy-efficient VLCs and low-cost LEDs are deployed indoors for illumination, realizing the novel concept of light fidelity (LiFi) networking [2], [5]. Consequently, green technologies based on VLC networks for next generation technologies are being developed.

VLC networks exhibit some challenges. For example, an optical AP does not provide broad spectrum communication because of the limitations of hardware technologies [7].

2169-3536 © 2019 IEEE. Translations and content mining are permitted for academic research only.
Personal use is also permitted, but republication/redistribution requires IEEE permission.
See http://www.ieee.org/publications_standards/publications/rights/index.html for more information.

An indoor ultra-dense network (UDN) based on VLC, which is a novel form of network management to address network density requirements, has high requirements that must be met [8]. The coverage of an optical AP is confined because of the line-of-sight propagation of visible light [9]. These challenges demand spectrum-efficient utilization to achieve high rates of traffic in local hotspot areas and meet the density requirements (such as high traffic density, high user equipment (UE) density, and high AP deployment) of UDNs in next-generation wireless communication [8]. To achieve spectrum-efficient utilization, we consider a user access scheme based on non-orthogonal multiple access (NOMA). Compared with orthogonal multiple access (OMA), NOMA can increase spectral efficiency by serving multiple users from the same resource block, such as a time slot, subcarrier, or spreading code [10]. The NOMA principle is a general framework and some proposed OMA schemes can be combined with NOMA. NOMA-VLC can continuously exploit the entire bandwidth for the time-frequency utilization with complete freedom to increase spectral efficiency. For UDN scenarios, the area throughput requirement may be as high as 20 Mbps/m^2. A public-private partnership for next-generation communication provides the performance evaluation models of use cases [11] and believes that UE deployment density in an indoor high-speed environment will be around five UEs per cell, and the deployment in a room of VLC system LEDs, whose coverage range is around 1–5 m, can be dense and arbitrary. When the number of users increases, the NOMA complexity problem may appear, but this is not the focus of this paper. The complexity of the power-domain and successive interference cancellation can be reduced when power-domain and other schemes are combined in NOMA [12], [13]. Reference [14] concluded that power-domain NOMA had the lowest complexity of all NOMA schemes in the power domain, code domain, and combined power-code domain. On the other hand, when using current and upcoming generations of processors for ubiquitous wireless sensor networks, the computational time complexity for NOMA message decoding is within acceptable limits [15]; it means that scalable low complexity resource allocation can be obtained using power-domain NOMA, which is highly desirable for machine–machine communication in 5G networks [16]. Therefore, in this paper, we focus on the power allocation strategy rationality of NOMA in a typical VLC scenario, and analyze the data rate performance of power allocation strategies with respect to VLC deployment.

There are two main approaches to optimizing NOMA power allocation: numerical search and strategic design. It is difficult to determine the optimal solution with either approach because this optimization problem is NP-hard [17]. The numerical search approach is expensive to compute, whereas using strategies is convenient for real-time processing. For strategic design, recent methods include the power law strategy (PLS) [18] and fractional transmit power allocation (FTPA) [19], [20], in which the assigned power decreases as the ratio of channel gains increases. In power-domain NOMA, the gain ratio power allocation (GRPA) scheme [18], which considers user channel conditions to ensure efficient and fair power allocation, was proposed to maximize the system throughput. In [18], a GRPA strategy based on a power law strategy that considers the VLC user channel conditions to ensure efficient and fair power allocation was presented. In [21], a normalized gain difference power allocation method based on PLS was proposed that exploits channel conditions in a multiple-input multiple-output (MIMO) VLC system. In [22], the PLS method of GRPA was improved to solve the problem of users with similar channels and accommodate a varying number of users in a MIMO-VLC system. In [23]–[25], various approaches including PLS and FTPA were compared, leading to a re-design of the power allocation strategy in NOMA-VLC networks.

However, the original PLS and FTPA approaches for NOMA GRPA that were first proposed for traditional radio frequency (RF) channels [26]–[28] may not be suitable for NOMA-VLC networks. When FTPA [19], [20] was first developed for radio frequency channels, the authors did not provide a rationale for this approach in closed-form solutions. Later, PLS [7] was proposed for VLC, but the authors did not provide a rationale for its use in VLC channels. When both FTPA and PLS were introduced into VLC, several studies [7], [21]–[24] did not present analytic evidence for the optimization of VLC power allocation. Until now, the performances attained by power allocation strategies have not been analyzed using closed-form solutions. Current VLC studies that introduce traditional PLS and FTPA may not fully consider the characteristics of VLC systems. Because indoor lighting is ubiquitous, both the purposes of illumination and communication (e.g., the height of an LED) in VLC networks must be considered. Therefore, this study addresses an important challenge: that GRPA should be designed in accordance with the characteristics of VLC channels so that power allocation coefficients are suitable for enhancing VLC system throughput in typical light source scenarios.

In this paper, a GRPA strategy that is suitable for VLC channels is designed. The contributions of this paper are listed as follows.

- Because of the difficulties involved in the direct analysis of complicated mathematical NOMA-VLC throughput forms, an alternative bound based on VLC channels is proposed for comparing candidate GRPA strategies. In addition, an improved FTPA strategy is designed by revising the power-counting coefficients within GRPA.
- For LED heights greater than 1 m, the proposed GRPA strategy yields a local extremum solution based on our proposed alternative bound, which is proved using the maximum-minimum criterion and Karush–Kuhn–Tucker conditions.
- For LED heights smaller than 1 m, the proposed GRPA strategy cannot maintain the system throughput based on visible light channels. However, a necessary but not

sufficient condition under which the proposed GRPA outperforms a previous method is derived.
- To analyze the throughput performance of the GRPA strategy, the experiments verify the compactness of the alternative bound for fitting the original NOMA-VLC GRPA target asymptotically. Furthermore, the relationship between GRPA and indoor VLC deployment is revealed by the experimental results, which are consistent with the theoretical derivations.

II. SYSTEM MODEL

A. INDOOR VLC SCENARIO

There are several indoor VLC scenarios, including ceiling-illumination, workbench-illumination, and display-illumination scenarios. We discuss these scenarios using examples in the following.

- Ceiling-illumination scenario: an optical AP or LED is fixed on the ceiling of a room or compartment. This scenario commonly exists in offices, apartments, airports, and subways. To ensure the minimum lighting requirements for a large number of users, this case is widely used in crowded or brightly lit places. Hence, the height of the installed LED is commonly increased to widen the coverage of illumination.
- Workbench-illumination scenario: an optical AP or LED could be deployed on a table or between the ceiling and users. This scenario commonly exists on workbenches and platforms for intelligent devices. In the workbench illumination scenario, the concept of a user may not be limited to a human user. Moreover, intelligent devices such as intelligent sound boxes and virtual reality equipment could become VLC receivers. Hence, users in this VLC scenario are generalized to include intelligent networking UEs involved in machine–machine communication.
- Display-illumination scenario: an optical AP or visible-light transmitter could be a display screen. With the popularization of smartphones equipped with high definition cameras and displays with high resolution, VLC can provide optical camera communication, which is performed between the display and a camera. The most common application of a display–camera communication link is the use of a mobile phone to scan visible-light frames for extracting codes or other information. Moreover, unobtrusive communication between a display and camera that is imperceptible to human eyes is a good opportunity for covert advertising.

Previous researchers have explored $\Phi_{1/2}$ (the semi-angle of the LED) and Ψ_{FOV} (the width of the field of vision (FOV) angle at the PD receiver), which are important factors in VLC scenarios. However, LED deployment includes the height of the LED, which may also affect the power allocation of indoor NOMA-VLC users. It has been noted that various VLC cell formations have remained to a large extent unexplored [9]. Furthermore, the effect of one important parameter in VLC cell deployment, LED height, on NOMA-VLC power allocation has not been yet discussed.

Let the distance between the LED and received plane be denoted by L [m]. In this study, we consider two cases based on height that occur in the above scenarios and that have different mathematical power allocation characteristics for NOMA-VLC networks.

- Case 1 ($L > 1$): this case commonly exists in crowded lighting areas. For example, in the ceiling-illumination scenario of a railway station or airport, the illuminants are deployed on the ceiling or hanging over the heads of the people. Without loss of generality, to guarantee both sufficient and economical illumination, the height of the LED between the transmitted and received planes is commonly greater than 1 m.
- Case 2 ($L \leq 1$): this case commonly exists in slanted and horizontal lighting areas. For example, in the workbench-illumination scenario, there could be several intelligent devices on the workbench that perform the machine–machine communication. In the display-illumination scenario, the customers use optical camera communication to scan information about the display or advertising wall at close range. Without loss of generality, to meet the requirements for special functionality, the distance between the transmitted and received planes may be less than 1 m.

Sometimes, an illumination scenario might not just be one of the two cases, because both may synchronously exist. For example, in the illumination scenario of a living room, the ceiling illumination belongs to the first case of and the bed lamp illumination belongs to the second case. In contrast, it is possible that the case of $L \leq 1$ may be used by multiple users, such as multiple devices held by multiple users standing in a semicircle and scanning a quick response code from a display.

In the following sections, we reveal the relationship between these cases and power allocation strategies for NOMA-VLC.

B. VLC CHANNELS

The entire coverage of a single AP, such as an LED, is defined as a cell of a VLC network. The users within a VLC cell use a photo diode (PD) as the VLC signal receiver. The indoor VLC signal model can be modelled using a Lambertian radiation model [29]. Considering that the VLC signal in the line-of-sight path is the main energy component, as shown in Fig. 1, we denote the VLC channel gain for the k-th user follows.

$$h_k = \frac{A(M+1)\,T}{2\pi d_k^2}\cos^m(\phi_k)\cos(\psi_k)\,g(\psi_k) \tag{1}$$

In (1), M is the order of Lambertian emission, A is the physical area of the PD detector, d_k is the distance between an LED transmitter and the PD receiver of the k-th user, ϕ_k is the angle of irradiance of the k-th user, ψ_k is the angle of incidence of the k-th user, T is a constant for the optical filter gain, and $g(\psi_k)$ is the gain of the optical concentrator of the

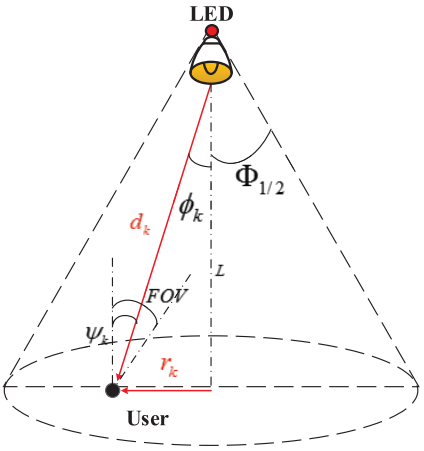

FIGURE 1. VLC channel model.

k-th user. In addition, m and $g(\psi_k)$ are respectively given by

$$M = -\frac{1}{\log_2\left(\cos\left(\Phi_{1/2}\right)\right)} \tag{2}$$

and

$$g(\psi_k) = \begin{cases} \dfrac{n^2}{\sin^2(\Psi_{FOV})}, & 0 \le \psi_k \le \Psi_{FOV} \\ 0, & \psi_k > \Psi_{FOV}. \end{cases} \tag{3}$$

Further, $\Phi_{1/2}$ is the semi-angle of the LED, Ψ_{FOV} is the width of the FOV angle at the PD receiver, and n is a constant for the refractive index. In summary, (1) indicates that a decrease in FOV leads to a decrease in user coverage [9], [25].

According to [30], if $\rho = \frac{Ag(\psi_k)T}{2\pi}$ and $d_k = \sqrt{r_k^2 + L^2}$, (3) can be transformed into

$$h_k = \frac{\rho\,(M+1)\,L^{M+1}}{\left(r_k^2 + L^2\right)^{\frac{M+3}{2}}}, \tag{4}$$

where L is the height of the LED. When the indoor user scenario is given, the LED lighting parameters are determined, for example, the lighting angles $\Phi_{1/2}$ and Ψ_{FOV} are certain, leading to a constant ρ. If the height of the LED and ρ are fixed, it is clear that the VLC channel gain is only dependent on user distance.

C. GRPA OF NOMA-VLC

When on-off keying and intensity modulation with direct detection are used in the transmitter and receiver, the received signal y_k transmitted from the LED to the $k-$th NOMA-VLC user is indicated by

$$y_k = \gamma_{oe} P_t h_k \sum_{i=1}^{K} a_i x_i + N_k, \tag{5}$$

where γ_{oe} is an optical-electrical conversion efficiency constant, P_t is the transmitted optical signal power, h_k is the VLC channel gain of the k-th user, a_i is the power allocation factor, x_i is the on-off keying signal, K is the number of total users, and N_k denotes the zero-mean Gaussian noise. Note that [31] considers that noise is caused by different independent sources and hence an intensity-modulation with direct-detection channel can be regarded as an additive white Gaussian noise channel.

Assume that $P_r = \gamma_{oe} P_t$ denotes the received signal power, which can be normalized. In GRPA for NOMA, the channel gains of the users can be listed in increasing order, e.g., $h_1 < h_2 < \cdots < h_k < \cdots < h_K$, whereas $a_1 > a_2 > \cdots > a_k > \cdots > a_K$. When successive interference cancellation is used, the signal to interference plus noise ratio (SINR) for the k-th NOMA-VLC user is calculated as follows, where N_0 is a constant noise power spectral density and B is a constant VLC bandwidth.

$$SINR_k = \frac{(h_k a_k)^2}{\sum_{i=k+1}^{K} (h_k a_i)^2 + N_0 B} \tag{6}$$

However, no exact closed-form expression for the VLC channel capacity has yet been established because of the different constraints of the input VLC signals [31]. In other words, the achievable data rate or capacity of a VLC channel remains controversial.

In this paper, we consider that

$$R_k(h_k, a_k) = \log_2\left(1 + \frac{(h_k a_k)^2}{\sum_{i=k+1}^{K} (h_k a_i)^2 + N_0 B}\right) \tag{7}$$

can be used to measure the equivalent VLC user data rate [9], [25], [30]. We provide several reasons for this assertion as follows.

- Reference [32] notes that the research modelling commonly includes Gaussian channels, which are suitable for modelling short-range VLC. Hence, an additive white Gaussian channel can be adopted in VLC channel models. Because there is no exact closed-form expression for VLC channel capacity, several tight capacity bounds are a more practical approach to determine the channel capacity in VLC performance analysis. Hence, it is better to derive the upper and lower bounds of a VLC system capacity because of the difficulty of accurate analytic expression [31], [32].
- Reference [33] noted that the maximizing input distribution is Gaussian for the Gaussian channel, which results in a channel capacity that is given by Shannon's theorem. Although Shannon's theorem is not appropriate for measuring the capacity, it can be considered for measuring the user data rate as a lower bound. As long as it is an accessible bound, proving that our strategy reaches a bound that the previous strategy does not reach, the comparison can still be taken into account.
- Two situations for VLC capacity are derived: one with inter-symbol interference (ISI) and one without ISI (ISI-free). If the average power constraint is commonly

assumed, the lower bound formulas of user data rate in ISI [34], [35] and ISI-free [31], [32], [36], [37] are respectively

$$R \geq \frac{B}{2}\log_2\left(1+\frac{1}{2\pi e}SINR\right) \tag{8}$$

and

$$R \geq \frac{B}{2}\log_2\left(1+\frac{e}{2\pi}SNR\right). \tag{9}$$

We note that e and π are constants, and SNR is the signal-to-noise ratio. Although (8) and (9) have different physical meanings, the consistency of these mathematical forms to a certain extent reflects that both have some common laws in their derivation. For example, both (8) and (9) can be regarded as having the uniform mathematical form of

$$R \geq \frac{B}{2}\log_2\left(1+\eta SINR\right), \tag{10}$$

where η is a determined value.

NOMA utilizes the whole available bandwidth and its efficiency can be normalized. We can regard the bandwidth as a common factor that can be extracted, and a constant η ensures that the power allocation strategy applies to other expressions of VLC channel capacity. Hence, we can use Shannon's theorem for convenience when establishing mathematical equivalence.

Finally, under the constraint of $\sum_{k\in[1,K]} a_k = 1$, the optimization target of GRPA, which achieves the maximum system throughput, is given as

$$\arg\max_{a_1,\cdots,a_k,\cdots,a_K} \sum_{k=1}^{K} R_k\left(h_k, a_k\right). \tag{11}$$

D. GRPA STRATEGY

Because of the NP-hardness of power allocation in NOMA [17], the mathematical form of the optimization target does not yield an analytical solution. Hence, a strategic design is a convenient approach for centralized control. This approach can flexibly handle the channel status information of all users.

Two GRPA strategies have been developed: PLS and FTPA.

- PLS: If a_k^{PLS} denotes the k-th user using PLS, the power allocation scheme based on PLS is expressed using the following two expressions:

$$a_k^{PLS} = \left(\frac{h_1}{h_k}\right)^k a_{k-1}^{PLS} \tag{12}$$

and

$$a_k^{PLS} = \frac{\prod_{i=1}^{k}\left(\frac{h_1}{h_i}\right)^k}{\sum_{k=1}^{K}\left(\prod_{i=1}^{k}\left(\frac{h_1}{h_i}\right)^k\right)}. \tag{13}$$

Note that the power counting of $(\frac{h_1}{h_i})$ is involved in the order of the user, which varies exponentially.

- FTPA: If a_k^{FTPA} denotes the k-th user using FTPA, the power allocation scheme based on FTPA can be expressed as

$$a_k^{FTPA} = \frac{\left(h_k^2\right)^{-\alpha}}{\sum_{i=1}^{K}\left(h_k^2\right)^{-\alpha}}, \tag{14}$$

where $0 \leq \alpha \leq 1$.

In this paper, we revise the FTPA and propose the improved fractional strategy (IFS). We reframe the channel proportions and eliminate the limitation of $0 \leq \alpha \leq 1$, as follows:

$$a_k^{IFS} = \frac{\left(\frac{h_1}{h_k}\right)^{\beta}}{\sum_{i=1}^{K}\left(\frac{h_1}{h_i}\right)^{\beta}}. \tag{15}$$

Here, β is not limited in the range $[0, 1]$ and not only relevant to the order of the user. In the following section, we prove that (15) with a certain $\beta > 0$ can reach a locally optimum solution for the NOMA-VLC system throughput.

III. ALTERNATIVE LOWER BOUND FOR NOMA-VLC THROUGHPUT

The system throughput of a NOMA-VLC network includes the sum of all user data rates. If the bandwidth utilization is normalized in NOMA and $R_k \triangleq \log_2(S_K)$, the original target of the throughput can be denoted as $\log_2(S_K)$, where S_K is calculated as follows.

$$S_K = \left[\left(1+\frac{(h_K a_K)^2}{N_0 B}\right)\prod_{k=1}^{K-1}\left(1+\frac{(h_k a_k)^2}{N_0 B+\sum_{i=k+1}^{K}(h_k a_i)^2}\right)\right] \tag{16}$$

However, because of the NP-hard nature of NOMA power allocation, the mathematical forms of NOMA-VLC throughput are too complicated for direct analysis. To evaluate the performance of the VLC user data rate for NOMA, for mathematical convenience, we present an alternative lower bound, which is the asymptotic lower bound of (16) based on VLC channels and is

$$S_K' = \left(1+\frac{\sum_{k=1}^{K}(h_k a_k)^2}{N_0 B}\right). \tag{17}$$

The asymptotic properties of (17) were proved in our previous study [25]. In this paper, we prove the compactness between (16) and (17) for VLC channels. If the LED location is given, the channel gain order of the users (i.e., $h_1 < \cdots < h_k < \cdots < h_K$) is based on the order of their radii (i.e., $r_1 > \cdots > r_k > \cdots > r_K$).

- For the two-user case: if (2) denotes the order of Lambertian emission M, we define $\theta = M + 3$. Because of the positive nature of (2), it is clear that $\theta > 1$. The upper difference between the capacity and alternative bound is given in the following equation, which is bounded and asymptotic to zero.

$$\begin{aligned}
&\frac{S_2 - S'_2}{S_2 - 1} \\
&= \frac{(h_1 a_1 a_2)^2 \left(h_2^2 - h_1^2\right)}{\left(h_1^2 a_1^2 + h_1^2 a_2^2\right)(h_2 a_2)^2 + \left(h_1^2 a_1^2 + h_2^2 a_2^2\right) N_0 B} \\
&\leq \frac{(h_1 a_1 a_2)^2 \left(h_2^2 - h_1^2\right)}{\left[(h_1 a_1)^2 + (h_1 a_2)^2\right]\left[(h_2 a_2)^2 + N_0 B\right]} \\
&\leq \frac{a_1^2}{a_1^2 + a_2^2}\left[1 - \left(\frac{h_1}{h_2}\right)^2\right] \leq \left[1 - \left(\frac{r_2^2 + L^2}{r_1^2 + L^2}\right)^{\theta}\right]
\end{aligned} \tag{18}$$

- Three-user case: If $\Theta_1 \triangleq (h_1 a_2)^2 + (h_1 a_3)^2 + N_0 B$ and $\Theta_2 \triangleq (h_2 a_2)^2 + (h_2 a_3)^2 + N_0 B$, it is clear that $N_0 B < \Theta_1 \leq \Theta_2$. If $\Theta_3 \triangleq N_0 B + (h_2 a_3)^2$ and $\Theta_4 \triangleq N_0 B + (h_3 a_3)^2$, then $N_0 B < \Theta_3 \leq \Theta_4$ is given. When $\Theta_5 \triangleq (h_1 a_1)^2 + (h_2 a_2)^2 + (h_3 a_3)^2$, a similar mathematical form indicating the bounded difference is obtained as follows.

$$\begin{aligned}
&\frac{S_3 - S'_3}{S_3 - 1} \\
&= 1 - \frac{\Theta_1 \Theta_3 \Theta_5}{(h_3 a_3)^2 \Theta_1 \Theta_3 + \left[(h_1 a_1)^2 \Theta_2 + (h_2 a_2)^2 \Theta_1\right]\Theta_4} \\
&\leq 1 - \frac{\Theta_1 \Theta_3 \Theta_5}{\Theta_2 \Theta_4 \Theta_5} \underset{(19a)}{\leq} 1 - \frac{(h_2 a_3)^2 \left[(h_1 a_2)^2 + (h_1 a_3)^2\right]}{(h_3 a_3)^2 \left[(h_2 a_2)^2 + (h_2 a_3)^2\right]} \\
&\leq 1 - \left(\frac{h_1}{h_3}\right)^2 = \left[1 - \left(\frac{r_3^2 + L^2}{r_1^2 + L^2}\right)^{\theta}\right]
\end{aligned} \tag{19}$$

Note that the demonstration of (19a) is equal to the demonstration of (20), where (20a) is supported by $N_0 B < \Theta_1 \leq \Theta_2$ and $N_0 B < \Theta_3 \leq \Theta_4$. Hence, (21) proves (19$a$).

$$\begin{aligned}
&1 - \frac{\Theta_1 \Theta_3 \Theta_5}{\Theta_2 \Theta_4 \Theta_5} \\
&\leq 1 - \frac{(h_2 a_3)^2 \left[(h_1 a_2)^2 + (h_1 a_3)^2\right]}{(h_3 a_3)^2 \left[(h_2 a_2)^2 + (h_2 a_3)^2\right]} \\
&\Leftrightarrow \frac{\Theta_1 \Theta_3}{\Theta_2 \Theta_4} - \frac{(\Theta_1 - N_0 B)(\Theta_3 - N_0 B)}{(\Theta_2 - N_0 B)(\Theta_4 - N_0 B)} \geq 0 \\
&\underset{(20a)}{\Leftrightarrow} \Theta_1 \Theta_3 (\Theta_2 - N_0 B)(\Theta_4 - N_0 B) \\
&\quad - \Theta_2 \Theta_4 (\Theta_1 - N_0 B)(\Theta_3 - N_0 B) \geq 0
\end{aligned} \tag{20}$$

(20a)

$$\begin{aligned}
&= \left(h_2^2 - h_1^2\right)\left(h_2 h_3 a_3^2\right)^2 \left(a_2^2 + a_3^2\right) \\
&\quad + \left(h_3^2 - h_2^2\right)(h_1 h_2 a_3)^2 \left(a_2^2 + a_3^2\right)^2 \\
&\quad + N_0 B \left(h_3^2 - h_1^2\right)(h_2 a_3)^2 \left(a_2^2 + a_3^2\right) \geq 0
\end{aligned} \tag{21}$$

- Multi-user case: We obtain

$$\frac{S_k - S'_k}{S_k - 1} \leq 1 - \left(\frac{h_1}{h_k}\right)^2 = \left[1 - \left(\frac{r_k^2 + L^2}{r_1^2 + L^2}\right)^{\theta}\right] \tag{22}$$

based on a relaxed upper bound difference in the N-user case, which indicates that our alternative bound retains its fitting behavior.

References [13] and [25] reflect the conclusion that the system throughput encounters an improvement bottleneck in the cell deployment when the number of users tends to saturation. When the number of users is sufficiently high, all the users in a single cell performing NOMA jointly cause strong signal interference in S_k. Hence, when the number of users is sufficiently high, we have $S_{k+1} \approx S_k$ and $S'_{k+1} \geq S'_k$. To prove that (22) with S_k is applicable to the N-user case, we use mathematical induction, which yields (23) to prove the S_{k+1} case.

$$\begin{aligned}
\frac{S_{k+1} - S'_{k+1}}{S_{k+1} - 1} &\leq \frac{S_k - S'_k}{S_k - 1} \leq 1 - \left(\frac{h_1}{h_k}\right)^2 \\
&\leq 1 - \left(\frac{h_1}{h_{k+1}}\right)^2
\end{aligned} \tag{23}$$

As the introduction indicates, the coverage of indoor VLC AP is more limited than that of RF. When the number of users increases, the difference in the radii among the VLC users may also decrease, which causes (22) to be bounded by zero.

IV. GRPA STRATEGY ANALYSIS FOR TWO CASES

The previous section indicates that the alternative bound can be used as an approximate target to evaluate the performance of the NOMA-VLC throughput. In the following section, we analyze the power allocation strategy based on this alternative bound in NOMA-VLC networks. We note that the constants 1 and $N_0 B$ are certain. Hence, the analysis based on (17) is equal to

$$S'_K = \left(1 + \frac{C_K}{N_0 B}\right), C_K = \sum_{k=1}^{K} (h_k a_k)^2. \tag{24}$$

The PLS of (13) and IFS of (15) are substituted into the C_K of the alternative bound as follows. Let us assume the order of users $v_k = k$ and the symbol $u_k = \sum_{i=2}^{k} v_i, K \geq k \geq 2$. Note that the initialization of v_k and u_k with $k = 1$ is denoted as $v_1 = u_1 = 1$. When $d_k = \sqrt{r_k^2 + L^2}$ and $D_k = \left(\sqrt{r_k^2 + L^2}\right)^{\theta} = d_k^{\theta}$, the main component C_K of the system throughput in PLS and IFS can be respectively

$$\frac{\partial\left(C_K^{IFS}\right)^{-1}}{\partial D_i}=\frac{2D_i^{2\beta-3}\left(\sum_{i=1}^{K}D_i^{\beta}\right)+2\beta\left[\sum_{j\neq i}^{j\in[1,K]}D_j^{\beta}D_i^{\beta-1}\left(D_j^{\beta-2}-D_i^{\beta-2}\right)\right]}{\left(\sum_{i=1}^{K}D_i^{2\beta-2}\right)^{2}\left(\sum_{i=1}^{K}D_i^{\beta}\right)^{-1}} \tag{32}$$

calculated using

$$C_K^{PLS}=\frac{D_1^{2u_K-2u_1}+\sum_{k=2}^{K}\left[D_1^{2u_K-2u_k}\left(\prod_{i=2}^{k-1}D_i^{2v_k}\right)D_k^{2v_k-2}\right]}{\left(D_1^{u_K}+\sum_{k=2}^{K}\left[D_1^{u_K-u_k}\left(\prod_{i=2}^{k}D_i^{v_k}\right)\right]\right)^{2}} \tag{25}$$

and

$$C_K^{IFS}=\frac{\sum_{k=1}^{K}D_k^{2\beta-2}}{\left(\sum_{k=1}^{K}D_k^{\beta}\right)^{2}}. \tag{26}$$

It is clear that $\max_a S'_K \Leftrightarrow \max_a C_K$.

A. CASE OF L > 1

Without loss of generality, $d_k > 1$ in this case. For this case, [25] proved that the average user data rate in IFS is better than that in PLS, and compared the two strategies alone. However, this study did not determine the conditions for optimality nor the optimal degree of IFS.

Due to the variety of possible LED deployments and power allocation factors that affect system throughput, the maximum-minimum criterion is used for the quality of service (QoS) guarantee in NOMA-VLC networks [38]–[40]. When the alternative lower bound of (17) is used, the power allocation optimization of system throughput for the QoS guarantee can be transformed into

$$\max_{a_k}\min_{d_k}\left(S'_K\right)=\max_{a_k}\min_{d_k}\left(1+\frac{\sum_{k=1}^{K}(h_ka_k)^2}{N_0B}\right),$$
$$s.t.\ \sum_{k=1}^{K}a_k=P_t,\ 0<a_k<\delta_k,\quad \forall k\le K. \tag{27}$$

Note that the constant term and N_0B are fixed, so that

$$\max_{a_k}\min_{d_k}\left(C_K\right)\le\min_{d_k}\max_{a_k}\sum_{k=1}^{K}(h_ka_k)^2 \tag{28}$$

can be the equivalent target of (27), for which the constraints are unchanged.

Commonly, indoor VLC networks are deployed in a predefined scenario, where h is known. If the cell deployment is given, (28) can ignore the variation of h_k and we can analyze the local optimum of $\max_{a_k}\sum_{k=1}^{K}(h_ka_k)^2$. If we obtain the minimum optimum of $\max_{a_k}\sum_{k=1}^{K}(h_ka_k)^2$, this extremum still approximates our target $\max_{a_k}\min_{d_k}\sum_{k=1}^{K}(h_ka_k)^2$, which mathematically and practically guarantees the validity of our demonstrations. Hence, a Lagrangian formulation can be expressed as follows:

$$Lag=\sum_{k=1}^{K}(h_ka_k)^2+\lambda\left(\sum_{k=1}^{K}a_k-P_t\right)+\sum_{k=1}^{K}\left[\mu_k\left(a_k-\delta_k\right)\right]-\sum_{k=1}^{K}\varepsilon_ka_k \tag{29}$$

and the partial derivative is derived as

$$\frac{\partial Lag}{\partial a_k}=2h_k^2a_k+\lambda+\mu_k-\varepsilon_k,$$
$$\frac{\partial Lag}{\partial\lambda}=\sum_{k=1}^{K}a_k-P_t, \tag{30}$$

where $\mu_k\left(a_k-\delta_k\right)=0$ and $\varepsilon_ka_k=0$. Finally, we obtain

$$\lambda=\frac{-P_t}{\sum_{k=1}^{K}\frac{1}{2h_k^2}}$$
$$a_k=\frac{-\lambda}{2h_k^2}=P_t\frac{\frac{1}{h_k^2}}{\sum_{k=1}^{K}\frac{1}{h_k^2}}=P_ta_k^{IFS(\beta=2)} \tag{31}$$

to indicate that $a_k^{IFS(\beta=2)}$ is the approximate solution for a local extremum. It is clear that (31) satisfies the Karush–Kuhn–Tucker conditions.

In this case, IFS with $\beta=2$ is a locally optimal solution for indoor NOMA-VLC networks. If the monotonicity analysis of $\left(C_K^{IFS}\right)$ in (32), as shown at the top of this page, is performed, when $\beta=2$, (32) yields (33), which indicates that an increase of $d_i\in[1,+\infty)$ cause an increase in $\left(C_K^{IFS}\right)^{-1}$ (i.e., a decrease of C_K^{IFS}). Therefore, the system throughput performance of IFS degrades as d_i increases.

$$\frac{\partial\left(C_K^{IFS}\right)^{-1}}{\partial D_i}=\frac{2D_i}{\sum_{i=1}^{K}D_i^2} \tag{33}$$

B. CASE OF $L \leq 1$

Without loss of generality $0 < d_k < 1$ in this case, so the data rate of IFS may not be greater than that of PLS. Hence, the pre-conditions that make the system throughput of IFS better than that of PLS are discussed.

Because the domain of β has been extended, the critical value is $\beta = 1$ for PLS, FTPA, and IFS. When $d_i \in (0, 1]$ and $\beta = 1$, if it is desired to have a higher data rate for IFS than for PLS, the target can be described as $(C_K^{IFS} - C_K^{PLS}) > 0$.

Let us assume that $C_K^{PLS} \triangleq \frac{Q_1(\boldsymbol{D})}{Q_2(\boldsymbol{D})}$ and $C_K^{IFS} \triangleq \frac{Q_3(\boldsymbol{D})}{Q_4(\boldsymbol{D})}$, where the numerators and denominators are indicated in

$$\begin{aligned} Q_1(\boldsymbol{D}) &= D_1^{2u_K - 2u_1} + \sum_{k=2}^{K} \left[D_1^{2u_K - 2u_k} \left(\prod_{i=2}^{k-1} D_i^{2v_k} \right) D_k^{2v_k - 2} \right] \\ Q_2(\boldsymbol{D}) &= \left(D_1^{u_K} + \sum_{k=2}^{K} \left[D_1^{u_K - u_k} \left(\prod_{i=2}^{k} D_i^{v_k} \right) \right] \right)^2 \\ Q_3(\boldsymbol{D}) &= \sum_{k=1}^{K} D_k^{2\beta - 2} \\ Q_4(\boldsymbol{D}) &= \left(\sum_{k=1}^{K} D_k^{\beta} \right)^2. \end{aligned} \tag{34}$$

For example, Q_1 denotes $Q_1(\boldsymbol{D}) \triangleq Q_1(D_1, \cdots, D_k, \cdots, D_K)$. Hence, the target of $(C_K^{IFS} - C_K^{PLS}) > 0$ requires $(Q_3 Q_2 - Q_4 Q_1) > 0$ under the constraints of $d_i \in (0, 1]$ and $\beta = 1$.

If $\beta = 1$, Q_3 is equal to K and the target of $(Q_3 Q_2 - Q_4 Q_1) > 0$ can be derived as

$$\begin{aligned} 0 < Q_3 Q_2 - Q_4 Q_1 &= K Q_2 - Q_4 Q_1 \\ &\leq K Q_2(\|\boldsymbol{D}\|_{\max}) - Q_4(\|\boldsymbol{D}\|_{\min}) Q_1(\|\boldsymbol{D}\|_{\max}), \end{aligned} \tag{35}$$

where $\|\boldsymbol{D}\|_{\min}$ means $\forall D_i = \min\left(d_1^{\theta}, d_2^{\theta}, \cdots, d_K^{\theta}\right), i \in [1, K]$.

In $Q_1(\boldsymbol{D})$ of (34), $u_k = \sum_{i=2}^{k} v_i, K \geq k \geq 2$. If we re-define $u_K^{\dagger} \triangleq u_K - u_{K-1} = v_K$, a novel $Q_1^{\dagger}(\|\boldsymbol{D}\|_{\max})$ can be obtained, where $Q_1^{\dagger}(\|\boldsymbol{D}\|_{\max}) \triangleq Q_1(\|\boldsymbol{D}\|_{\max})|_{u_K^{\dagger} \triangleq v_K}$. If we can prove

$$Q_1^{\dagger}(\|\boldsymbol{D}\|_{\max}) \geq \sqrt{Q_2(\|\boldsymbol{D}\|_{\max})} \geq Q_1(\|\boldsymbol{D}\|_{\max}) \tag{36}$$

and

$$Q_2(\|\boldsymbol{D}\|_{\max}) \geq Q_1^{\dagger}(\|\boldsymbol{D}\|_{\max}) Q_1(\|\boldsymbol{D}\|_{\max}), \tag{37}$$

we can transform (35) into

$$\begin{aligned} &K Q_2(\|\boldsymbol{D}\|_{\max}) - Q_4(\|\boldsymbol{D}\|_{\min}) Q_1(\|\boldsymbol{D}\|_{\max}) \\ &\geq \left[K Q_1^{\dagger}(\|\boldsymbol{D}\|_{\max}) - Q_4(\|\boldsymbol{D}\|_{\min}) \right] Q_1(\|\boldsymbol{D}\|_{\max}) \geq 0. \end{aligned} \tag{38}$$

If (38) is satisfied, (35) is true. Hence, the necessary but not sufficient condition that indicates that IFS performs better can be given by

$$K > \frac{\ln \|\boldsymbol{D}\|_{\max}}{\ln \|\boldsymbol{D}\|_{\min}} + 1. \tag{39}$$

The proofs of (36) and (37) are as follows.

- Proof of (36): An indoor NOMA-VLC network serves at least two users, which means $u_k \geq 2$ with $k \geq 2$. Because $\theta > 1$, $d_i \in (0, 1]$, $u_1 = 1$, and $u_{k \geq 2} \geq 2$, $D^{2u_k - 2} \leq D^{u_k}$ is given by

$$D^{2u_k - 2} - D^{u_k} = D^{u_k} \left(D^{u_k - 2} - 1 \right) \leq 0. \tag{40}$$

  Hence, each item of $\sqrt{Q_2(\boldsymbol{D})}$ is greater than the corresponding item of $Q_1(\boldsymbol{D})$. Similarly, according to mathematical induction, $D^{2v_k - 2} \geq D^{u_k}$ can be obtained, which means $Q_1^{\dagger}(\|\boldsymbol{D}\|_{\max}) \geq \sqrt{Q_2(\|\boldsymbol{D}\|_{\max})}$.
- Proof of (37): combined with the proof of (36),

$$K^2 \left(\|D\|_{\max} \right)^{2u_K} - K^2 \left(\|D\|_{\max} \right)^{2v_K - 2} \left(\|D\|_{\max} \right)^{2u_K - 2} \geq 0 \tag{41}$$

  is given. Hence, (37) is proved.

V. SIMULATION AND NUMERICAL RESULTS

The simulation parameters are listed in Table 1 and reported in [25], [29], and [30]. The purpose of each experiment is as follows.

TABLE 1. Experimental parameters.

Symbol	Name	Value
γ_{oe}	Optical-electrical conversion efficiency	$0.53A/W$
$\Phi_{1/2}$	Semi-angle of the LED	$60°$
Ψ_{FOV}	Field of vision (FOV) of the receiver	$60°$
A	Physical photosensitive area of the receiver	$10^{-4}m^2$
T_f	Optical filter gain	1
n	Refractive index	1.5
M	Order of Lambertian emission	1
$g(\psi_k)$	Optical concentrator gain ($\psi_k = \Psi_{FOV}$)	3
L	Height of the LED at the ceiling	$2.0m$–$2.4\ m$
L	Height of the LED on the workbench	$0.2m$–$0.4\ m$
N_0	Noise power spectral density	$10^{-19}A^2/Hz$
B	System bandwidth	$30MHz$
P_t	Transmitted optical signal power	$9W$
Room	Room size	$6m \times 6m$

- Analysis of the bound compactness: although the alternative lower bound is asymptotic to the capacity, the compactness or gap between the two bounds is evaluated in this experiment. Furthermore, we propose an empirical law for fitting the original system throughput for convenience, which can be used for a numerical search method.
- Analysis of the LED height: the height of the LED is one parameter of indoor VLC cell deployment. In this experiment, we discover that the different heights affect the performance of power allocation schemes. Furthermore, the optimum property and the comeback advantages of GRPA strategies for NOMA-VLC are evaluated in this experiment.
- Analysis of the lighting angles: the semi-angle $\Phi_{1/2}$ and FOV jointly influence indoor VLC cell performance. Increasing $\Phi_{1/2}$ and Ψ_{FOV} achieves seamless coverage, but worse receiving conditions may exist. In this

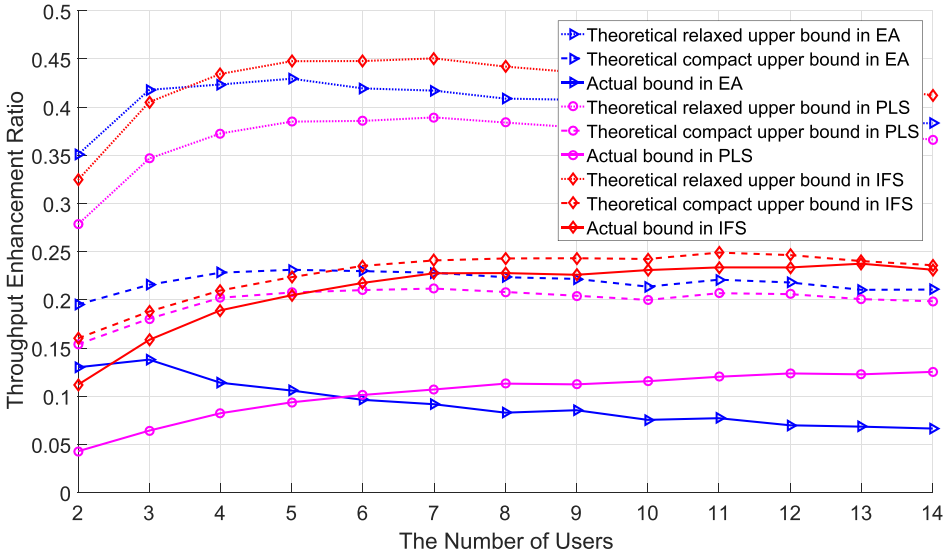

FIGURE 2. System throughput enhancement ratio based on relaxed upper, compact upper, and actual bounds.

experiment, the conditions under which interference and coverage occur are determined.

The average user data rate (AUDR) is used to evaluate the system throughput. The throughput enhancement ratio reflects the gap between lower bound and capacity.

A. BEHAVIOR OF THE ALTERNATIVE BOUND

We denote the actual enhancement as $(S_k - S'_k)$ and the theoretical enhancement as the upper bound of $(S_k - S'_k)$. For normalized system throughput, Fig. 2 shows that the decrease in the enhancement ratio difference between the two bounds reflects the compactness of the alternative bound. Compared with the equal allocation (EA) values of NOMA and PLS, our proposed IFS method achieves the best enhancement ratio. Moreover, the theoretical relaxed upper bound derived in (17) tracks the performance and has a similar behavior.

For VLC channels, we propose the empirical law

$$\frac{S_k - S'_k}{S_k - 1} \leq \frac{1}{1 + \left(\frac{h_{k-1}}{h_k}\right)^2} \left(1 - \sqrt{\frac{h_1}{h_k}}\right) \tag{42}$$

to improve the compactness of our proposed alternative bound for the convenience of numerical fitting to PLS. Fig. 2 shows that for the compact upper bound based on (42), the theoretical enhancement of our strategy approaches the actual enhancement. These results indicate that the increase from the alternative bound to the actual target bound is tightly fitted by the proposed empirical law.

B. HEIGHT OF LED IN ILLUMINATION CASES

In the ceiling-illumination case, when $L > 1$ m and $\beta = 2$, Fig. 3 shows that the AUDR of our proposed IFS is better than that of PLS. Moreover, both the AUDR of IFS and PLS decrease as L increases. For $L > 1$ m, $L = 2.4$ m leads to the worst AUDR performance for IFS, whereas it is greater than the best AUDR performance of PLS at $L = 2$ m. This indicates that the proposed IFS approach supports longer distance communication than PLS without degrading the AUDR.

Furthermore, the variety of power counting in the ceiling-illumination case is analyzed in Fig. 4. When the parameters are set as listed in Table 1 except for $\beta > 1$ and $L = 1.1$ m, Fig. 4 indicates that the extremum $\beta = 2$ exists in both the actual and alternative bounds. Because of its NP hardness, original target (16) may not be directly analyzed. However, our proposed alternative bound with (31) can yields the local extremum solution, which indicates that our proposed bound is suitable for indicating the functional behavior of the original problem.

In the workbench-illumination case, when $0 < L < 1$ m and $\beta = 1$, Fig. 3 shows the situations of $L < 1$ m. Because of the FOV constraint in Table 1, the user distance may not exceed 1 m. We notice that the AUDR values of the GRPA strategies have their own maxima and minima. However, we can use the condition (39) to explain this. The uncertain advantages of our IFS in the workbench-illumination case are at the intersections between the IFS and PLS AUDR curves. When $\Phi_{1/2} = 60°$ and $\Psi_{FOV} = 60°$, we obtain $d_{\min} = L$ and $d_{\max} = 2L$. Given (39) and $L = 0.4$ m, the number of users is greater than six, for which can IFS achieve a better AUDR than PLS. When $L = 0.2$ m and $L = 0.3$ m, (39) coincides with the experimental results as well. This indicates that the theoretical conclusions in (39) are consistent with the experimental results in Fig. 3.

C. LIGHTING ANGLES IN ILLUMINATION CASES

When $\Phi_{1/2}$ and Ψ_{FOV} are varied, the AUDR of different lighting angles and GRPA schemes are compared. In Fig. 5, when Ψ_{FOV} is fixed, the decrease of $\Phi_{1/2}$ in 40°–60° causes

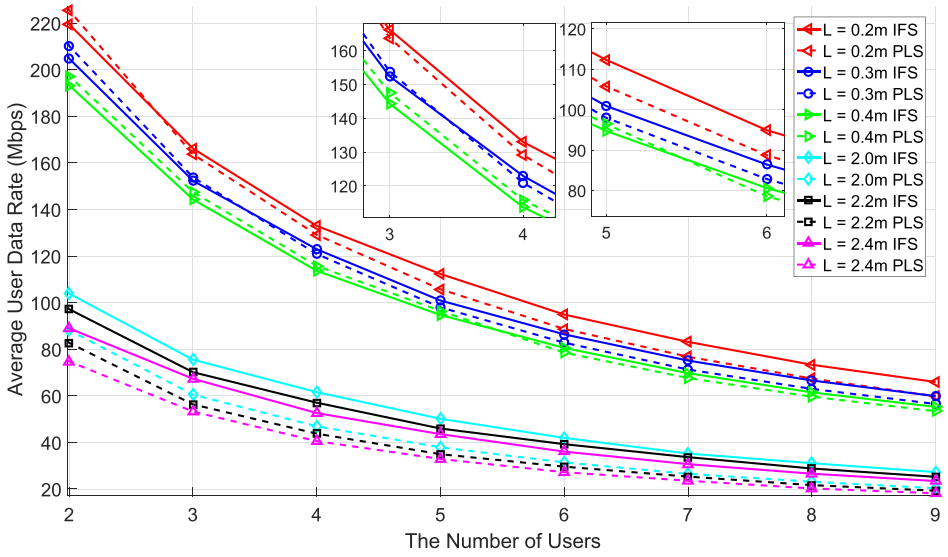

FIGURE 3. AUDR comparisons for different LED heights VLC illumination systems cases.

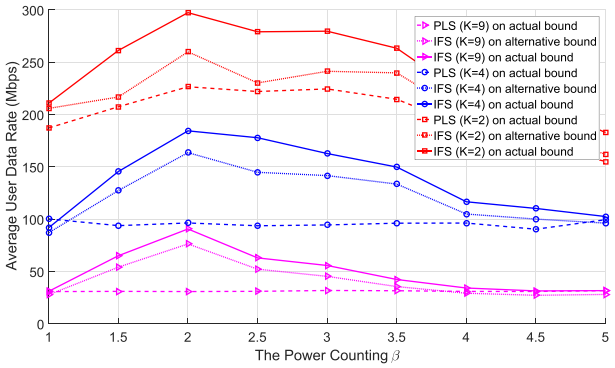

FIGURE 4. AUDR comparisons based on different values of power counting parameter β.

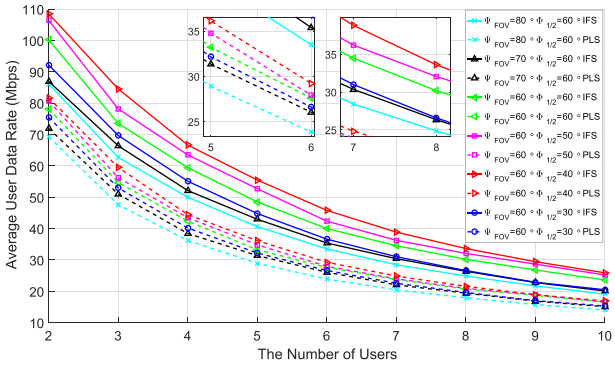

FIGURE 5. The AUDR comparison with varied $\Phi_{1/2}$ and Ψ_{FOV} among GRPA strategies.

the AUDR to increase. This indicates that the reduced semi-angle results in a concentration of the light beam, and visible-light energy is provided to users more centrally. However, when $30^\circ \leq \Phi_{1/2} \leq 40^\circ$, the AUDRs of IFS and PLS increase, which reflects the difference in monotonicity with regard to $40^\circ \leq \Phi_{1/2} \leq 60^\circ$. In contrast, when $\Phi_{1/2}$ is fixed, the decrease of Ψ_{FOV} causes $g(\psi_k)$ to increase, improving the VLC channel gains. For different pairs of $\Phi_{1/2}$ and Ψ_{FOV}, the decreasing monotonicity of AUDR is not altered when Ψ_{FOV} increases. This single variable control mode reflects that the optimum extremum of $\Phi_{1/2}$ appears, whereas Ψ_{FOV} does not reflect that.

In summary, the pair of $\Phi_{1/2} = 40^\circ$ and $\Psi_{FOV} = 60^\circ$ in IFS leads to the best AUDR, and an LED deployment with this pair of values is an appropriate layout in this scenario. Furthermore, when $\Phi_{1/2}$ is fixed, our strategy with smaller Ψ_{FOV} achieves a better AUDR than PLS does. Hence, our strategy is suitable for worse receiving conditions.

VI. CONCLUSION

Because of the complicated mathematical forms in the NOMA-VLC throughput, this paper presented an alternative bound to facilitate the comparison of GRPA strategies. The compactness between the alternative bound and actual capacity was analyzed using both analytic and numerical results. For the ceiling-illumination case, we demonstrated that our IFS approach is better than PLS with respect to AUDR. For the workbench-illumination case, the necessary conditions that are needed for our IFS approach to remain better is given by this paper. In future work, we will investigate a demonstration of the workbench-illumination case and the properties of our alternative bound. In addition, the scenario that involves a correlated channel deserves to be developed by us. References [22] considered the correlated-channel case with GRPA in NOMA-VLC, whereas our paper assumes that the channel correlation may be handled by another network scheme [41], such as space modulation [42], or in the code domain [14]. Although [41] indicated that users can completely remove interference if their channel gains are fully

correlated in NOMA, we believe that the correlated channel model leads to an accurate fitting analysis, and this belongs to a task for future work.

ACKNOWLEDGMENT

Doctor Siyu Tao appreciates the technical support of Doctor Yan-qun Tang and M.Phil. Xiangwei Bai, and feels grateful for valuable suggestions of Associate Professor Qing Li and anonymous reviewers.

REFERENCES

[1] Cisco, San Jose, CA, USA. *Cisco Visual Networking Index: Forecast and Methodology, 2016–2021*. Accessed: Nov. 26, 2018. [Online]. Available: https://www.cisco.com/c/en/us/solutions/collateral/service-provider/visual-networking-index-vni/complete-white-paper-c11-481360.html

[2] H. Haas, L. Yin, Y. Wang, and C. Chen, "What is LiFi?" *J. Lightw. Technol.*, vol. 34, no. 6, pp. 1533–1544, Dec. 15, 2015, doi: 10.1109/JLT.2015.2510021.

[3] S. Wu, H. Wang, and C.-H. Youn, "Visible light communications for 5G wireless networking systems: From fixed to mobile communications," *IEEE Netw.*, vol. 28, no. 6, pp. 41–45, Nov. 2014, doi: 10.1109/MNET.2014.6963803.

[4] IEEE, Piscataway, NJ, USA. *Light Communications for Wireless Local Area Networking*. Accessed: Jan. 26, 2019. [Online]. Available: https://futurenetworks.ieee.org/tech-focus/may-2018/light-communications-for-wireless-local-area-networking

[5] H. Haas, C. Chen, and D. O'Brien, "A guide to wireless networking by light," *Prog. Quantum Electron.*, vol. 55, pp. 88–111, Sep. 2017, doi: 10.1016/j.pquantelec.2017.06.003.

[6] W. Shaoen, H. Wang, and C.-H. Youn, "Visible light communications for 5G wireless networking systems: from fixed to mobile communications," *IEEE Netw.*, vol. 28, no. 6, pp. 41–45, Nov. 2014, doi: 10.1109/MNET.2014.6963803.

[7] H. Marshoud, V. M. Kapinas, G. K. Karagiannidis, and S. Muhaidat, "Non-orthogonal multiple access for visible light communications," *IEEE Photon. Technol. Lett.*, vol. 28, no. 1, pp. 51–54, Jan. 1, 2015, doi: 10.1109/LPT.2015.2479600.

[8] S. Chen, F. Qin, B. Hu, X. Li, and Z. Chen, "User-centric ultra-dense networks for 5G: Challenges, methodologies, and directions," *IEEE Wireless Commun.*, vol. 23, no. 2, pp. 78–85, Apr. 2016, doi: 10.1109/MWC.2016.7462488.

[9] X. Li, R. Zhang, J. Wang, and L. Hanzo, "Cell-centric and user-centric multi-user scheduling in visible light communication aided networks," in *Proc. IEEE Int. Conf. Commun.* London, U.K., Jun. 2015, pp. 5120–5125, doi: 10.1109/ICC.2015.7249136.

[10] Z. Ding, X. Lei, G. K. Karagiannidis, R. Schober, J. Yuan, and V. Bhargava, "A survey on non-orthogonal multiple access for 5G networks: Research challenges and future trends," *IEEE J. Sel. Areas Commun.*, vol. 35, no. 10, pp. 2181–2195, Oct. 2017, doi: 10.1109/JSAC.2017.2725519.

[11] K. Chandra, A. S. Marcano, S. M. Mumtaz, R. V. Prasad, and H. L. Christiansen, "Unveiling Capacity Gains in Ultradense Networks: Using mm-Wave NOMA," *IEEE Veh. Technol. Mag.*, vol. 13, no. 2 pp. 75–83, Jun. 2018, doi: 10.1109/MVT.2018.2814822.

[12] L. Dai, B. Wang, Y. Yuan, S. Han, C.-L. I, and Z. Wang, "Non-orthogonal multiple access for 5G: Solutions, challenges, opportunities, and future research trends," *IEEE Commun. Mag.*, vol. 53, no. 9, pp. 74–81, Sep. 2015, doi: 10.1109/MCOM.2015.7263349.

[13] S. M. R. Islam, N. Avazov, O. A. Dobre, and K.-S. Kwak, "Power-domain non-orthogonal multiple access (NOMA) in 5G systems: Potentials and challenges," *IEEE Commun. Surveys Tuts.*, vol. 19, no. 2, pp. 721–742, 2nd Quart., 2017, doi: 10.1109/COMST.2016.2621116.

[14] M. Moltafet, N. Mokari, M. R. Javan, H. Saeedi, and H. Pishro-Nik, "A new multiple access technique for 5G: Power domain sparse code multiple access (PSMA)," *IEEE Access*, vol. 6, pp. 747–759, 2018, doi: 10.1109/ACCESS.2017.2775338.

[15] A. Anwar, B.-C. Seet, and Z. Ding, "Non-orthogonal multiple access for ubiquitous wireless sensor networks," *Sensors*, vol. 18, no. 2, p. 516, 2018, doi: 10.3390/s18020516.

[16] E. Balevi and R. D. Gitlin, "Pareto optimization for uplink NOMA power control," in *Proc. IEEE Wireless Telecommun. Symp. (WTS)* Phoenix, AZ, USA, Apr. 2018, pp. 1–5 doi: 10.1109/WTS.2018.8363931.

[17] L. Lei, D. Yuan, C. K. Ho, and S. Sun, "Power and channel allocation for non-orthogonal multiple access in 5G systems: Tractability and computation," *IEEE Trans. Wireless Commun.*, vol. 15, no. 12, pp. 8580–8594, Dec. 2016, doi: 10.1109/TWC.2016.2616310.

[18] H. Marshoud, V. M. Kapinas, G. K. Karagiannidis, and S. Muhaidat, "Non-orthogonal multiple access for visible light communications," *IEEE Photon. Technol. Lett.*, vol. 28, no. 1, pp. 51–54, Jan. 1, 2016, doi: 10.1109/LPT.2015.2479600.

[19] Y. Saito, A. Benjebbour, Y. Kishiyama, and T. Nakamura, "System-level performance evaluation of downlink non-orthogonal multiple access," in *Proc. IEEE Int. Symposium Pers., Indoor, Mobile Radio Commun.* London, U.K., Sep. 2013, pp. 611–615, doi: 10.1109/PIMRC.2013.6666209.

[20] A. Benjebbovu, A. Li, Y. Saito, Y. Kishiyama, A. Harada, and T. Nakamura, "System-level performance of downlink NOMA for future LTE enhancements," in *IEEE Globecom Workshops* Atlanta, GA, USA, Dec. 2013, pp. 66–70, doi: 10.1109/GLOCOMW.2013.6824963.

[21] C. Chen, W.-De Zhong, H. Yang, and P. Du, "On the performance of MIMO-NOMA-based visible light communication systems," *IEEE Photon. Technol. Lett.*, vol. 30, no. 4, pp. 307–310, Feb. 15, 2018, doi: 10.1109/LPT.2017.2785964.

[22] R. Mitra and V. Bhatia, "Precoded Chebyshev-NLMS-based predistorter for nonlinear LED compensation in NOMA-VLC," *IEEE Trans. Commun.*, vol. 65, no. 11, pp. 4845–4856, Nov. 2017, doi: 10.1109/TCOMM.2017.2736548.

[23] J. Kejun, H. Li, B. Lijun, and Y. Caihong, "Indoor visible light communication system based on non-orthogonal multiple access," *Acta Opt. Sinica*, vol. 37, no. 8, p. 0806004, Aug. 2017, doi: 10.3788/AOS201737.0806004.

[24] H. Marshoud, S. Muhaidat, P. C. Sofotasios, S. Hussain, M. A. Imran, and B. S. Sharif, "Optical non-orthogonal multiple access for visible light communication," *IEEE Wireless Commun.*, vol. 25, no. 2, pp. 82–88, Apr. 2018, doi: .10.1109/MWC.2018.1700122.

[25] S. Tao, H. Yu, Q. Li, and Y. Tang, "Performance analysis of gain ratio power allocation strategies for non-orthogonal multiple access in indoor visible light communication networks," *EURASIP J. Wireless Commun. Netw.*, vol. 2018, no. 1, pp. 1–14, Jun. 2018, doi: 10.1186/s13638-018-1152-z.

[26] M.-R. Hojeij, J. Farah, C. A. Nour, and C. Douillard, "Resource allocation in downlink non-orthogonal multiple access (NOMA) for future radio access," in *Proc. IEEE Veh. Technol. Conf.* Glasgow, U.K., May 2015, pp. 1–6, doi: 10.1109/VTCSpring.2015.7146056.

[27] M. M. El-Sayed, A. S. Ibrahim, and M. M. Khairy, "Power allocation strategies for Non-Orthogonal Multiple Access," in *Proc. Int. Conf. Sel. Topics Mobile Wireless Netw.* Cairo, Egypt, 2016, pp. 1–6, doi: 10.1109/MoWNet.2016.7496633.

[28] M.-R. Hojeij, J. Farah, C. A. Nour, and C. Douillard, "New optimal and suboptimal resource allocation techniques for downlink non-orthogonal multiple access," *Wireless Pers. Commun.*, vol. 87, no. 3, pp. 837–867, Apr. 2016, doi: 10.1007/s11277-015-2629-2.

[29] T. Komine and M. Nakagawa, "Fundamental analysis for visible-light communication system using LED lights," *IEEE Trans. Consum. Electron.*, vol. 50, no. 1, pp. 100–107, Feb. 2014, doi: 10.1109/TCE.2004.1277847.

[30] L. Yin, W. O. Popoola, X. Wu, and H. Haas, "Performance evaluation of non-orthogonal multiple access in visible light communication," *IEEE Trans. Commun.*, vol. 64, no. 12, pp. 5162–5175, Dec. 2016, doi: 10.1109/TCOMM.2016.2612195.

[31] R. Jiang, Q. Wang, H. Haas, and Z. Wang, "Joint user association and power allocation for cell-free visible light communication networks," *IEEE J. Sel. Areas Commun.*, vol. 36, no. 1, pp. 136–148, Jan. 2018, doi: 10.1109/JSAC.2017.2774400.

[32] J.-Y. Wang, "Capacity analysis and constellation design in visible light communication systems," Ph.D. dissertation, School Inf. Sci. Eng., Nat. Mobile Commun. Res. Lab., Southeast Univ., Nanjing, China, Dec. 2015.

[33] A. Goldsmith, *Wireless Communications*. Cambridge, U.K.: Cambridge Univ. Press, 2005, pp. 92–93.

[34] H. Shen, Y. Deng, W. Xu, and C. Zhao, "Rate maximization for downlink multiuser visible light communications," *IEEE Access*, vol. 4, pp. 6567–6573, May 2017, doi: 10.1109/ACCESS.2016.2614598.

[35] J. Zhou and W. Zhang, "On the capacity of bandlimited optical intensity channels with Gaussian noise," *IEEE Trans. Commun.*, vol. 65, no. 6, pp. 2481–2493, Jun. 2017, doi: 10.1109/TCOMM.2017.2669966.

[36] A. Lapidoth, S. M. Moser, and M. A. Wigger, "On the capacity of free-space optical intensity channels," *IEEE Trans. Inf. Theory*, vol. 55, no. 10, pp. 4449–4461, Oct. 2009, doi: 10.1109/TIT.2009.2027522.
[37] L. Yin and H. Haas, "Physical-layer security in multiuser visible light communication networks," *IEEE J. Sel. Areas Commun.*, vol. 36, no.1, pp. 162–174, Jan. 2018, doi: 10.1109/JSAC.2017.2774429.
[38] T. V. Pham and A. T. Pham, "Max-min fairness and sum-rate maximization of MU-VLC local networks," in *Proc. IEEE Globecom Workshops (GC Wkshps),* San Diego, CA, USA, Dec. 2015, pp. 1–6, doi: 10.1109/GLOCOMW.2015.7414133.
[39] M. F. Hanif, Z. Ding, T. Ratnarajah, and G. K. Karagiannidis, "A minorization-maximization method for optimizing sum rate in the downlink of non-orthogonal multiple access systems," *IEEE Trans. Signal Process.*, vol. 64, no. 1, pp. 76–88, Jan. 2016, doi: 10.1109/TSP.2015.2480042.
[40] X. Zhang, Q. Gao, C. Gong, and Z. Xu, "User grouping and power allocation for NOMA visible light communication multi-cell networks," *IEEE Commun. Lett.*, vol. 21, no. 4, pp. 777–780, Apr. 2017, doi: 10.1109/LCOMM.2016.2642921.
[41] S. Ali, E. Hossain, and D. I. Kim, "Non-orthogonal multiple access (NOMA) for downlink multiuser MIMO systems: User clustering, beamforming, and power allocation," *IEEE Access*, vol. 5, pp. 565–577, Mar. 2017, doi: 10.1109/ACCESS.2016.2646183.
[42] A. Nuwanpriya, S.-W. Ho, and C. S. Chen, "Indoor MIMO visible light communications: Novel angle diversity receivers for mobile users," *IEEE J. Sel. Areas Commun.*, vol. 33, no. 9, pp. 1780–1792, Sep. 2015, doi: 10.1109/JSAC.2015.2432514.

SIYU TAO (S'17) received the B.S. degree from the Beijing Institute of Technology, in 2013, and the M.S. degree from the National Digital Switching System Engineering and Technological Center, in 2016, where he is currently pursuing the Ph.D. degree. His research interests include visible light communication and network protocol analysis.

HONGYI YU received the Ph.D. degree from Xidian University, in 1998. He is currently a Professor with the National Digital Switching System Engineering and Technological Center. His research interests include visible light communication networks, wireless communication, and signal processing.

QING LI received the M.S. and Ph.D. degrees from the National Digital Switching System Engineering and Technological Center, in 2003 and 2009, respectively. She is currently an Associate Professor to work on the wireless communication network and protocol reverse engineering.

YANQUN TANG received the B.S., M.S., and Ph.D. degrees from the School of Electronic Science and Engineering, National University of Defense Technology, China, in 2007, 2009, and 2013, respectively. He is currently a Lecturer with the National Digital Switching System Engineering and Technological Center. His research interests include physical layer security and visible light communication.